Journal of Biomolecular NMR (2006) 35: 209–223
DOI 10.1007/s10858-006-9033-x
© Springer 2006

Article

Dissecting non-canonical interactions in frameshift-stimulating mRNA pseudoknots

Peter V. Cornish[a,d], David P. Giedroc[a] & Mirko Hennig[b,c,*]
[a]*Department of Biochemistry and Biophysics, 2128 TAMU, Texas A&M University, College Station, TX 77843-2128, USA;* [b]*Department of Molecular Biology, The Scripps Research Institute, MB33, 10550 North Torrey Pines Road, La Jolla, CA 92037, USA;* [c]*Department of Biochemistry and Molecular Biology, Medical University of South Carolina, 173 Ashley Ave, PO Box 250509, Charleston, SC 29425, USA;* [d]*Department of Physics, University of Illinois at Urbana-Champaign, 1110 West Green Street, Urbana, IL 61801-3080, USA*

Received 7 March 2006; Accepted 17 May 2006

Key words: RNA pseudoknots, hydrogen bonds, *J*(N,N) scalar couplings, *J*(H,N) scalar couplings, ^{15}N chemical shifts, adiabatic pulses

Abstract

A variety of powerful NMR experiments have been introduced over the last few years that allow for the direct identification of different combinations of donor and acceptor atoms involved in hydrogen bonds in biomolecules. This ability to directly observe tertiary structural hydrogen bonds in solution tremendously facilitates structural studies of nucleic acids. We show here that an adiabatic HNN-COSY pulse scheme permits observation and measurement of *J*(N,N) couplings for nitrogen sites that are separated by up to 140 ppm in a single experiment at a proton resonance frequency of 500 MHz. Crucial hydrogen bond acceptor sites in nucleic acids, such as cytidine N3 nitrogens, can be unambiguously identified even in the absence of detectable H41 and H42 amino protons using a novel triple-resonance two-dimensional experiment, denoted H5(C5C4)N3. The unambiguous identification of amino nitrogen donor and aromatic nitrogen acceptor sites associated with both major groove as well as minor groove triple base pairs reveal the details of hydrogen bonding networks that stabilize the complex architecture of frameshift-stimulating mRNA pseudoknots. Another key tertiary interaction involving a 2′-OH hydroxyl proton that donates a hydrogen bond to an aromatic nitrogen acceptor in a *cis* Watson–Crick/sugar edge interaction can also be directly detected using a quantitative *J*(H,N) ^{1}H,^{15}N-HSQC experiment.

Introduction

The three-dimensional structures of RNA molecules dictate their vast range of biological functions. Tertiary structural interactions between elements of regular secondary structure such as A-form helices play an integral role in determining these three-dimensional folds of RNAs. Complex hydrogen bonding networks are ubiquitously stabilizing for both regular secondary as well as RNA tertiary structures (Jeffrey and Saenger, 1991). Traditionally, hydrogen bonds are inferred indirectly from the proximity of donor and acceptor functional groups during structural refinement using either NMR or X-ray crystallographic techniques. The observation of scalar couplings across hydrogen bonds in both DNA (Pervushin et al., 1998) and RNA (Dingley and Grzesiek, 1998) in Watson–Crick base pairs provides direct

*To whom correspondence should be addressed. E-mail: hennig@musc.edu

evidence for hydrogen bonding, a unique advantage to NMR. Canonical base-pair hydrogen bonding of the Watson–Crick type is fundamental in all biological processes where nucleic acids are involved. Several groups have also reported measuring scalar couplings across hydrogen bonds in non-canonical base pairs and in tertiary structural interactions (Dingley et al., 1999; Majumdar et al., 1999a; Majumdar et al., 1999b; Wohnert et al., 1999; Dingley et al., 2000; Hennig and Williamson, 2000; Liu et al., 2000b).

Moderate to weak hydrogen bonds constitute a unique type of interatomic interaction with typical energies ranging from 2 to 10 kcal mol^{-1}, which is intermediate between covalent bonds and Van der Waals forces. The partially covalent character of hydrogen bonds gives rise to measurable scalar spin–spin couplings of e.g. the type ^{h2}J(N,N) and ^{h1}J(H,N) that represent important additional NMR parameters for the structure determination of nucleic acids in solution (Dingley and Grzesiek, 1998; Pervushin et al., 1998). The unambiguous identification of hydrogen bonds is important in nucleic acid structure determination particularly for tertiary structural interactions; in the absence of such direct measurements, hydrogen-bonding partners can be misassigned, which will subsequently impact the precision of the resulting structure. In addition to the unambiguous determination of donor and acceptor nuclei involved in hydrogen bond formation, the magnitude of the ^{h}J(D,A) couplings reports on the hydrogen bond geometry and could potentially provide more precise distance information for structure calculations in the case of non-bifurcated, rigid donor and acceptor configurations. Scalar coupling interactions across hydrogen bonds follow the same electron-mediated polarization mechanism as their covalent counterparts and the Fermi-contact term between proton-donor (D) and acceptor (A) nuclei typically represents the dominant contribution (Del Bene et al., 1999; Dingley et al., 1999; Scheurer and Bruschweiler, 1999; Benedict et al., 2000; Barfield et al., 2001; Wilkens et al., 2002). Quantum mechanical calculations show that the appearance of *trans* hydrogen bond scalar couplings is associated with common molecular orbitals extending over both proton donor D and acceptor A nuclei; they predict a correlation of the distance, r(D...A), between the coupled nuclei and the size of the scalar coupling, ^{h}J(D,A). However, caution should be exercised in extracting r(D...A) from experimental scalar couplings ^{h}J(D,A). Observed scalar couplings across hydrogen bonds also report on hydrogen bond strength, but seemingly clear-cut correlations between geometry and energy of hydrogen bonds are only recently emerging (Kawahara et al., 2003).

RNA pseudoknots were first recognized as prevalent RNA folding motifs in the tRNA-like structure found at the 3′ end of turnip yellow mosaic virus (TYMV) genomic RNA (Pleij et al., 1985), the solution structure of which was determined by NMR spectroscopy (Kolk et al., 1998). Pseudoknotted RNA structures are also involved in programmed −1 ribosomal frameshifting (PRF); a mechanism in which *cis*-acting elements in the mRNA direct elongating ribosomes to shift reading frame by 1 base in the 5′ direction. The −1 PRF signal typically consists of three discrete parts: a slippery sequence, a linker region, and a downstream stimulatory region of stable mRNA structure (Giedroc et al., 2000). In many cases, this stimulatory RNA structure has been shown to be an H-type (Hairpin) pseudoknot, a stem-loop structure where nucleotides from the 3′ end fold back to form an additional stem 2 (S2) through base pairing with the loop 1 (L1) (Pleij, 1994). The resulting two stems S1 and S2 stack in a near coaxial geometry to form a quasi-continuous helix with one continuous and one discontinuous strand (Du et al., 1996; Puglisi et al., 1990). The first structure of a functional −1 PRF signal was the NMR structure of the mouse mammary tumor virus (MMTV) frameshift-stimulating pseudoknot (Shen and Tinoco, 1995).

The luteoviral −1 frameshift-stimulating RNA pseudoknots from sugarcane yellow leaf virus (ScYLV) and pea enation mosaic virus-1 (PEMV-1) are stabilized by intricate tertiary structural hydrogen bonding interactions including a major groove base triple and several minor groove base triples (Figure 1). The major groove L1 – S2 base triple contains a protonated cytidine *trans* Watson–Crick/Hoogsteen base pair shown to be essential for efficient frameshift stimulation and pseudoknot stability (Figure 2A) (Nixon et al., 2002a; Nixon et al., 2002b; Cornish et al., 2005). The two minor groove L2 – S1 base triples in the ScYLV RNA, C27·(C14-G7) and A24·(C15-G6), and in the PEMV-1 RNA, A27·(C15-G8) and A25·(C16-G7), nearest the helical junction are also characteristic of luteoviral pseudoknots (Fig-

ure 2B, C) (Su et al., 1999; Cornish et al., 2005; Nixon et al., 2002b; Pallan et al., 2005). However, the ScYLV RNA pseudoknot is the first structurally characterized RNA pseudoknot with cytidine as the terminal nucleotide in L2 (Cornish et al., 2005). The ScYLV RNA pseudoknot has two additional L2 – S1 minor groove interactions not found in the PEMV-1 RNA (Figure 2C, D). The NMR spectroscopic analysis of the ScYLV and PEMV-1 RNA pseudoknots presented here provides insight into these critical tertiary structural interactions and allows for the development of diagnostic spectral fingerprints, that might be used for the prediction of RNA tertiary structural interactions in other complex RNA molecules.

Experimental

Sample preparation

Both the uniformly ^{13}C,^{15}N-labeled ScYLV and PEMV-1 RNAs were produced by runoff transcription using SP6 RNA polymerase. Following ethanol precipitation, the RNAs were purified by denaturing PAGE and electroeluted. NMR samples were prepared by multiple rounds of ethanol precipitation into a final buffer of 10 mM phosphate (pH 6.0) containing 100 mM KCl, and 5.0 mM $MgCl_2$. The final sample concentrations were 0.9 mM for the ScYLV RNA and 1.0 mM for the PEMV-1 RNA in 500 µl H_2O/D_2O (90%/10%) unless otherwise indicated.

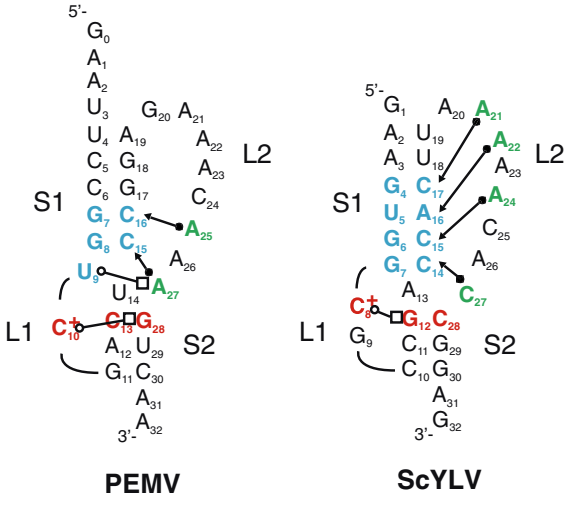

Figure 1. Schematic representations of the ScYLV and PEMV-1 mRNA pseudoknots. Tertiary structural interactions are represented by symbols as follows; *cis* Watson–Crick/sugar edge interaction (closed circle and triangle) and *trans* Watson–Crick/Hoogsteen interaction (open circle and square) (Leontis and Westhof, 2001). Residues not involved in tertiary structural interactions are shown in black.

NMR spectroscopy

NMR experiments were recorded on a four-channel Bruker Avance500 spectrometer equipped with an actively shielded z-gradient triple-resonance probe, at temperatures of either 298 or 288 K, unless otherwise stated. All spectra were processed using the NMRPipe program package (Delaglio et al., 1995). A solvent suppression filter was used in the ω_2 dimension to eliminate distortions from residual water prior to apodization with a Lorentz-to-Gauss window function. Data sets were zero-filled twice before Fourier transformation and only the downfield ^1H region of the spectra was retained. The ω_1 data were apodized with a 72° shifted sinebell window function and zero-filled prior to Fourier transformation. The absorptive part of the final 2D matrices were 1024 × 256 points for the adiabatic HNN-COSY, 1024 × 256 points for the two-bond ^2J(H,N) ^1H,^{15}N-HSQC, 2048 × 256 points for the quantitative J(H,N) ^1H, ^{15}N-HSQC, and 512 × 128 points for the H5(C5C4)N3 spectrum, respectively. Peak positions and intensities were determined using polynomial interpolation with Felix2000 (Accelrys, San Diego). All proton chemical shifts are referenced to external DSS and nitrogen shifts are referenced indirectly according to the chemical shift ratio (Wishart et al., 1995).

H5(C5C4)N3 experiment

A number of new NMR experiments have recently been introduced for RNA nucleobase resonance assignments (Fiala et al., 2004; Furtig et al., 2004; Wohnert et al., 2003). Here, we describe a new triple-resonance two-dimensional experiment for the unambiguous assignment of cytidine N3 nitrogen resonances, H5(C5C4)N3. The corresponding pulse sequence is shown in Figure 3A. The experiment identifies the N3 nitrogens of both pyrimidine bases, cytidine and uridine, by correlating them to intrabase non-exchangeable H5 proton resonances. Briefly, magnetization is transferred in an out-and-back fashion from the

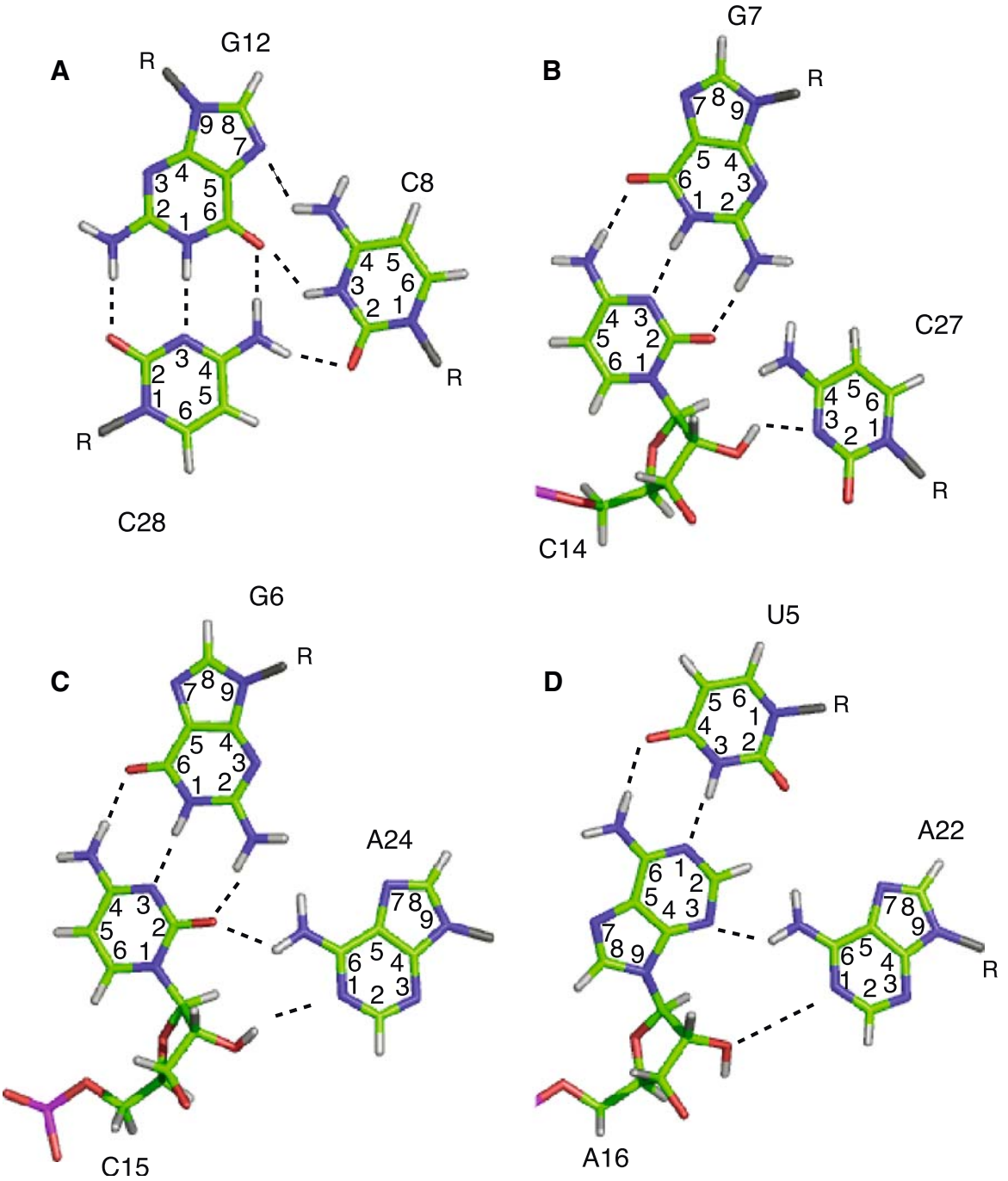

Figure 2. Tertiary structural interactions in the ScYLV RNA pseudoknot probed in this study. The previously published final ensemble of 20 structures (pdb code 1YG3) and the resulting average structure (1YG4) shown have been calculated without any loop L2-stem S1 hydrogen bonding restraints. Base ring atoms are numbered and dashed lines represent hydrogen bonding interactions. (A) Major groove L1-S2 *trans* Watson–Crick/Hoogsteen base pair, C8+·(G12-C28). (B) L2 – S1 minor groove *cis* Watson–Crick/sugar edge base pair, C27·(C14-G7). (C) L2 – S1 minor groove *cis* Watson–Crick/sugar edge base pair, A24·(C15-G6). This is identical to the A21·(C17-G4) *cis* Watson–Crick/sugar edge base pair, which is not shown. (D) L2 – S1 minor groove *cis* Watson–Crick/sugar edge base pair, A22·(A16-U5).

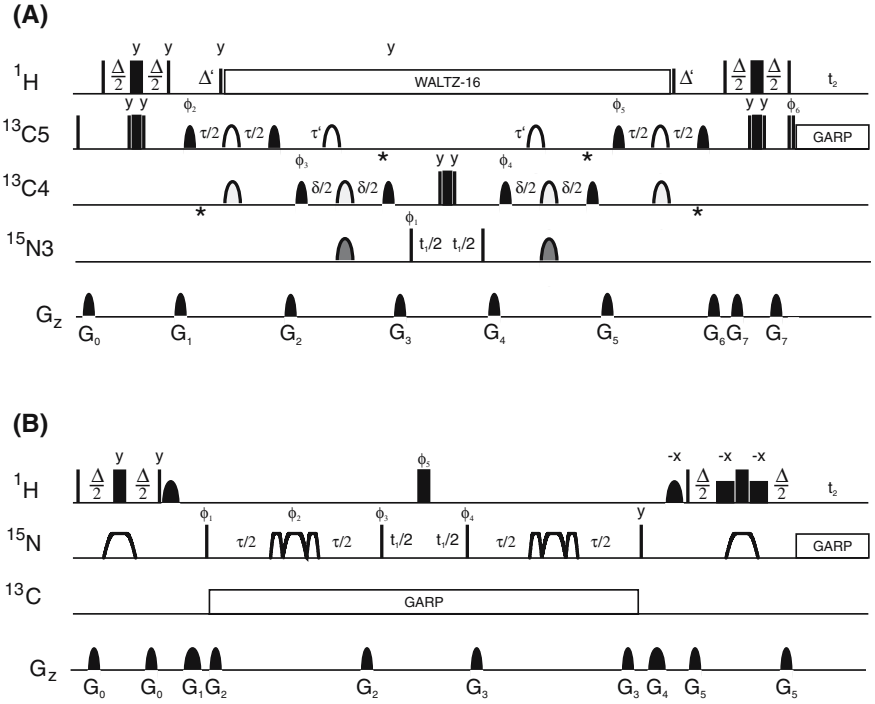

Figure 3. NMR experiments for pyrimidine N3 resonance assignment and quantitative measurement of scalar couplings across hydrogen bonds. Narrow and wide rectangles represent $\pi/2$- and π-pulses, respectively. All unmarked pulses have *x*-phase. (A) Pulse Sequence for the H5(C5C4)N3 experiment. Carrier positions were 196.1 ppm for ^{15}N3, 98.2 ppm for ^{13}C5, and 4.78 ppm for ^{1}H, respectively. All ^{1}H pulses were given on resonance for the water signal. High power proton pulses were applied with a field strength of 24.8 kHz. Proton decoupling was achieved using a 5.2 kHz WALTZ-16 decoupling field (Shaka et al., 1983) with 5.2 kHz flanking pulses on either side of the decoupling sequence. Shaped ^{13}C excitation pulses (black) were G4 Gaussian cascades (Emsley and Bodenhausen, 1992) with a duration of 2048 μs. Every second G4 was applied time-reversed. The ^{13}C carrier position was changed to 168.1 ppm (^{13}C4) during the pulse sequence prior to the pulse labeled with ϕ_3 and returned to 98.2 ppm prior to the pulse labeled with phase ϕ_5. Bandselective ^{13}C5 inversion pulses in the middle of the de- and refocusing delays τ had a Q3 shape (Emsley and Bodenhausen, 1992) and a length of 1024 μs (white). Bandselective ^{13}C4 inversion pulses in the middle of the de- and refocusing delays δ had a Q3 shape and a length of 1536 μs (light gray). Off-resonant selective Q3 inversion pulses of durations 1024 μs (white, C5) and 1536 μs (light gray, C4) during ^{13}C5-^{13}C4 INEPT transfers were implemented as phase-modulated pulses. Bloch–Siegert phase shifts during the ^{13}C5-^{13}C4 transfers were compensated by the application of a second off-resonance Q3 Gaussian cascade (denoted *) separated from the first one by an on-resonance selective Q3 inversion pulse (Emsley and Bodenhausen, 1990). ^{13}C decoupling during acquisition employed a 2.5 kHz GARP field (Shaka et al., 1985), while high power ^{13}C pulses were applied with a field strength of 18.1 kHz. High power ^{15}N pulses were applied with a field strength of 7.9 kHz while the bandselective inversion of ^{15}N3 magnetization during the de- and refocusing delays δ was achieved using Q3 Gaussian cascades of duration $\tau_p = 1024$ μs (dark gray). The phase cycling is $\phi_1 = x, -x$, $\phi_2 = 2(x), 2(-x)$, $\phi_3 = 4(x), 4(-x)$, $\phi_4 = 8(x), 8(-x)$, $\phi_5 = 16(x), 16(-x)$, $\phi_6 = 32(x), 32(-x)$, receiver = $x, -x, -x, x, 2(-x, x, x, -x), x, -x, -x, x, -x, x, x, -x, 2(x, -x, -x, x), -x, x, x, -x$. Quadrature detection was obtained in the t_2 dimension by altering ϕ_1 according to States-TPPI (Marion et al., 1989). Delay durations were $\Delta = 2.5$ ms, $\Delta' = 2.8$ ms, $\tau = 3.4$ ms, $\tau' = 4.5$ ms, and $\delta = 50$ ms, respectively. Sine-shaped Gradient durations and amplitudes were: G_0 1.0 ms (16.5 G/cm); G_1 1.0 ms (19.25 G/cm); G_2 1.0 ms (−3.3 G/cm); G_3 1.0 ms (2.75 G/cm); G_4 1.0 ms (−5.5 G/cm); G_5 1.0 ms (4.95 G/cm); G_6 1.0 ms (−24.75 G/cm); G_7 0.5 ms (30.25 G/cm). Proton decoupling was interrupted prior to the application of gradients G_2, G_3, G_4 and G_5. (B) Pulse Sequence for the quantitative, adiabatic HNN-COSY. Carrier positions were 147.6 ppm for ^{15}N, and 4.78 ppm for ^{1}H, respectively. All ^{1}H pulses were given on resonance for the water signal. High power proton pulses were applied with a field strength of 24.8 kHz. Shaped Gauss $\pi/2$-pulses with a duration of 2 ms were employed after the first and before the reverse INEPT to optimize water flip-back (Grzesiek and Bax, 1993). The reverse ^{15}N-^{1}H INEPT transfer has been adapted to include a WATERGATE solvent suppression scheme (Piotto et al., 1992). The high power proton π-pulse is flanked by two selective square pulses with durations of 1 ms.^{15}N decoupling during acquisition employed a 1.4 kHz GARP field (Shaka et al., 1985), while high power ^{15}N pulses were applied with a field strength of 7.9 kHz. The inversion of ^{15}N magnetization during the first and the final INEPT transfer step Δ is achieved using single smoothed amplitude CHIRP (sinusoidal smoothing over initial and final 30%) (Bohlen and Bodenhausen, 1993) adiabatic pulses of duration $\tau_p = 700$ μs with linear frequency sweeps of 30 kHz and peak *rf*-amplitudes of $(\gamma B_1/2\pi)^{max} = 5.1$ kHz. Expansion of the single CHIRP inversion pulse into composite, time-symmetric adiabatic [CHIRP-21,42,21] (Hwang et al., 1997) pulses of total length $\tau_p = 2.8$ ms allows broadband refocusing of ^{15}N magnetization during the de- and refocusing periods τ. Carbon decoupling during the extended de- and refocusing periods τ was achieved using a 2.5 kHz GARP decoupling scheme (Shaka et al., 1985) centered at 110.6 ppm to suppress scalar relaxation of the second kind (Liu et al., 2000a). The phase cycling is $\phi_1 = x, -x$, $\phi_2 = x, -x$ $\phi_3 = 2(y), 2(-y)$, $\phi_4 = 4(x), 4(-x)$, $\phi_5 = 8(x), 8(-x)$, receiver = $x, -x$. Quadrature detection was obtained in the t_2 dimension by altering ϕ_1, ϕ_2, and ϕ_3 according to States-TPPI (Marion et al., 1989). The delays for the INEPT and ^{15}N,^{15}N de- and refocusing periods were $\Delta = 5.0$ ms and τ = 38–46 ms, respectively (see text). Sine-shaped Gradient durations and amplitudes were: G_0 0.5 ms (5.5 G/cm); G_1 1.0 ms (30.25 G/cm); G_2 0.5 ms (3.85 G/cm); G_3 0.5 ms (9.35 G/cm); G_4 1.0 ms (24.75 G/cm); G_5 0.5 ms (27.5 G/cm). Carbon decoupling was interrupted prior to the application of gradients G_2 and G_3.

H5 proton to the directly attached C5 carbon and subsequently relayed via consecutive C5–C4 and C4–N3 INEPT transfer steps to the N3 nitrogen. After following the reverse transfer pathway, magnetization is detected on the H5 protons. In order to minimize magnetization leakage to unwanted pathways, all transfer steps employ band selective C5, C4, and N3 pulses. However, the large number of transfer steps and, in some cases, small couplings involved in the relay of magnetization from the H5 proton to the N3 nitrogen will limit the utility of this experiments to RNA molecules with favorable relaxation properties, i.e. with molecular masses on the order of 15 kDa or less. In the case of cytidine, the very small heteronuclear, one-bond C4–N3 coupling ($|^1J$(C4,N3)$|\sim$ 3 to 4 Hz) (Fiala et al., 2004; Wijmenga and van Buuren, 1998) represents a major bottleneck for the magnetization transfer and therefore lowers the sensitivity of the experiment. The length of the corresponding transfer delay was empirically optimized to $\delta = 50$ ms, which represents the best compromise for the optimal theoretical value of $\delta = 1/2J$(C4,N3) and the minimization of occurring magnetization loss mainly caused by T_2-relaxation of the quaternary C4 carbon. The corresponding ^1J(C4,N3) scalar coupling is almost twice as large for uridines; consequently, all three possible H5-N3 correlations can be readily observed for uridines while only five out of nine correlations are detectable for cytidines (see Figure 4).

For the H5(C5C4)N3 experiment, 16 complex points were recorded with an acquisition time of 31.5 ms for ^{15}N (ω_1), and 256 complex points with an acquisition time of 93.6 ms for ^{1}H (ω_2). A repetition delay between transients of 1.5 s was used, with 512 scans per increment (total measuring time 8 h).

Quantitative adiabatic J(N,N) HNN-COSY

The simultaneous identification of nuclei involved in hydrogen bonds and quantification of corresponding ^2J(N,N) scalar couplings is hampered by the finite strength of the ^{15}N radio frequency (rf) pulses and the potentially wide chemical shift separation of far upfield donor and far downfield acceptor ^{15}N nuclei (chemical shift difference of up to 7.1 kHz at 500 MHz ^{1}H resonance frequency). This wide chemical shift separation renders the conventional HNN-COSY experiment inefficient for the detection of correlations between amino and aromatic nitrogens. In order to overcome this limitation, Majumdar and co-workers developed a heteronuclear H(N)N-COSY experiment to establish correlations across hydrogen bonds between amino N6 donor and aromatic N7 acceptor nitrogens in a DNA A-A mismatch (Majumdar et al., 1999a). In this pulse scheme, selective ^{15}N-pulses excite the amino and aromatic chemical shift ranges separately. They employed an additional CT-^{1}H,^{15}N-HSQC based spin–echo difference experiment to quantify the corresponding ^{h2}J(N6,N7) scalar couplings. Subsequently, an improved version, a pseudo-heteronuclear HNN-COSY experiment designed to detect both donor and acceptor chemical shifts in a single experiment, was presented by Grzesiek and co-workers to determine ^{h2}J(N2,N7) scalar couplings in a DNA G-quartet (Dingley et al., 2000). This elegant experiment relies on phase coherent, phase-modulated excitation $\pi/2$-pulses with minimal cross excitation of amino and aromatic nitrogen chemical shifts.

Adiabatic pulses provide an attractive alternative with respect to treating the different nitrogen nuclei as a (pseudo)-heteronuclear spin system for establishing correlations where the chemical shift range of interest is very large (Kupce, 2001). An adiabatic frequency sweep achieves broadband spin inversion very effectively without the need for strong rf-amplitudes. An added benefit of adiabatic pulses is their exceptional tolerance against rf-miscalibrations. Therefore, we replaced all critical rectangular π-pulses by adiabatic pulses in our improved adiabatic HNN-COSY experiment as shown in Figure 3B. We employed smoothed amplitude (sinusoidal smoothing over initial and final 30%), linear sweep (CHIRP) (Bohlen and Bodenhausen, 1993) adiabatic pulses of duration $\tau_p = 700$ μs with frequency sweeps of 30 kHz to achieve broadband inversion of all donor and acceptor ^{15}N nuclei. Simulations carried out with NMRSim (Bruker BioSpin GmbH, Rheinstetten) indicate that these adiabatic CHIRP inversion pulses cover a band of ± 8.1 kHz (≥95% inversion of initial M_z) which is more than adequate for a chemical shift difference of up to 7.1 kHz (^{1}H resonance frequency: 500 MHz) between amino and aromatic nitrogens in nucleic acids. This procedure is straightforward for inversion pulses

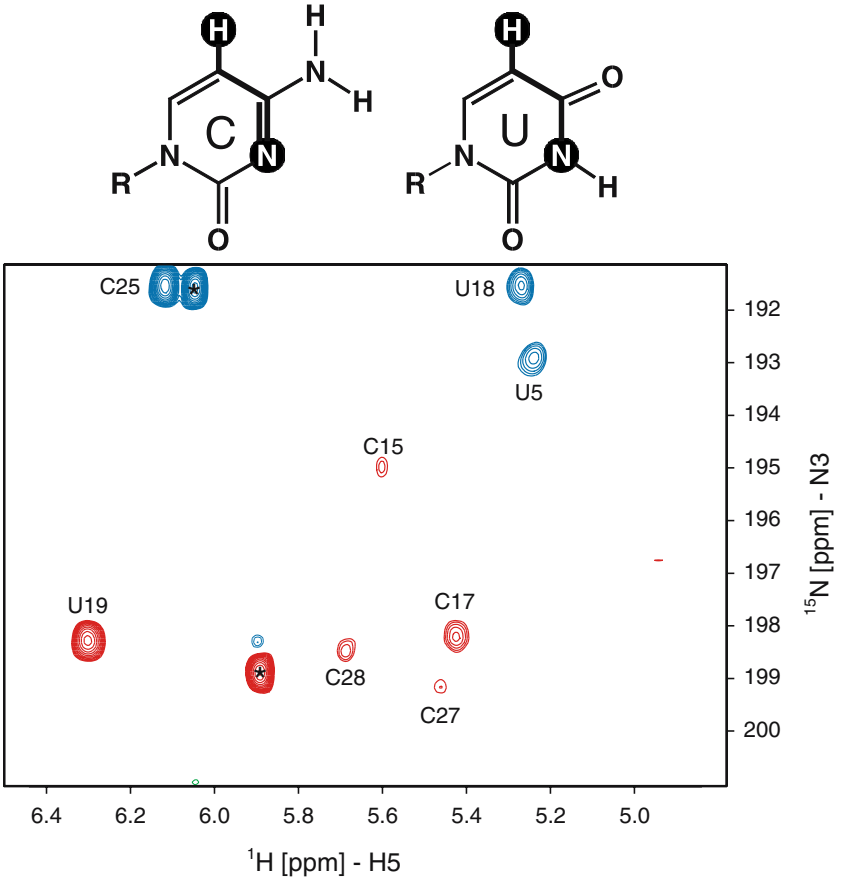

Figure 4. Pyrimidine nucleobases with correlated nuclei and magnetization transfer of the H5(C5C4)N3 experiment highlighted (acquired at 500 MHz (25 °C) for the ScYLV RNA). The two-dimensional spectrum was aquired such that some of the ^{15}N resonances are folded in ω_1 (^{15}N3) to improve digital resolution. Since the first t_1 point was half the dwell time, the folded and unfolded peaks have opposite signs (Bax et al., 1991; Zhu et al., 1993). Uracil N3 resonances are folded three times (−3*sw) in the ω_1 (^{15}N) dimension for U5 and U18 and four times (−4*sw) for U19. C25 is folded in once (+sw). Asterisks (*) represent peaks due to sample degradation.

during the INEPT ^{1}H—^{15}N transfers; however, it is more complicated to employ adiabatic pulses when magnetization requires refocusing. Single adiabatic pulses are not suitable refocusing elements because they produce undesirable phase rolls across the spectrum as a function of chemical shift offset. This introduced residual phase dispersion caused by a single adiabatic pulse shows a quadratic offset dependence. In order to overcome this limitation, we used composite adiabatic CHIRP pulses that efficiently eliminate the phase distortions by inverting the direction of spin precession. Following the nomenclature introduced by Garwood and coworkers, the applied composite, time-symmetric adiabatic pulse of total length $\tau_p = 2.8$ ms can be described as [CHIRP-21,42,21] (Hwang et al., 1997). No appreciable phase distortion can be detected within the ^{15}N bandwidth of >130 ppm shown in Figures 5 and 6 when using this combination of broadband adiabatic inversion and composite adiabatic refocusing pulses. It should be noted that the excitation of donor and acceptor ^{15}N nuclei at 500 MHz ^{1}H resonance frequency can be readily accomplished by conventional rectangular ^{15}N $\pi/2$-pulses of duration $\tau_p = 31.5$ μs exhibiting an excitation bandwidth of ±10.3 kHz (≥95% excitation of $M_{xy} = (M_x^2 + M_y^2)^{1/2}$ from initial M_z).

For the quantitative *J*-correlation adiabatic HNN-COSY spectrum, 64 complex points were recorded with an acquisition time of 14.8 ms for ^{15}N (ω_1), and 1024 complex points with an acquisition time of 93.5 ms for ^{1}H (ω_2). A repetition delay between transients of 1.5 s was used,

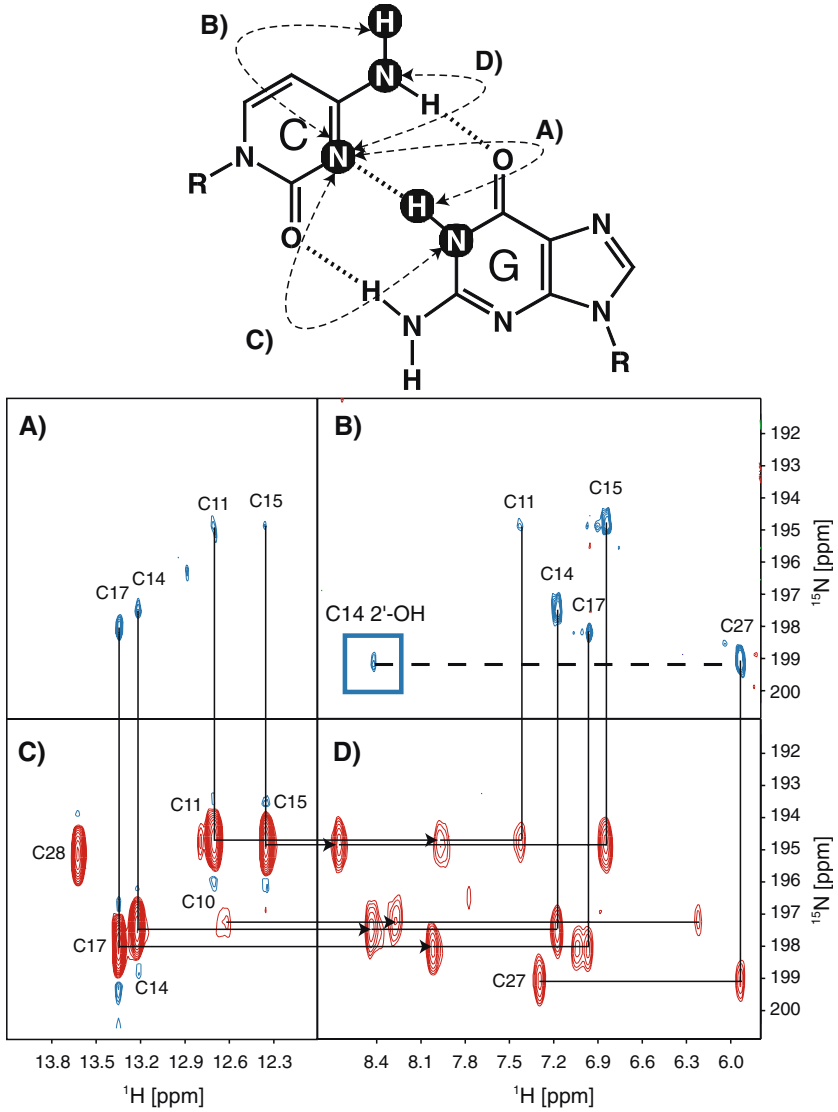

Figure 5. Watson–Crick G-C base pair with Cytidine N3 correlations highlighted by arrows. Quantitative J(H,N) ^{1}H,^{15}N-HSQC, recorded at 600 MHz, (A, B) and quantitative, adiabatic J(N,N) HNN-COSY (C, D) experiment, recorded at 500 MHz. (A) Cytidine N3 to guanosine H1 correlations mediated by ^{h1}J(H1,N3). (B) Cytidine N3 to cytidine amino H41 correlations mediated by ^{3}J(H41,N3). The boxed cross peak represents the C14 2′-OH to C27 N3 correlation mediated by ^{h1}J(2′-OH,N3), see Figure 2B. (C) Cytidine N3 to guanosine H1 correlations mediated by ^{h2}J(N1,N3). (D) Cytidine N3 to cytidine amino H41/2 correlations mediated by ^{2}J(N4,N3).

with 256 scans per increment (total measuring time 16 h).

Two-bond $^{2}J(H,N)$ $^{1}H,^{15}N$-HSQC

The large two-bond ^{2}J(H,N) scalar couplings within the purine bases allow reasonably efficient magnetization transfer during INEPT delays (Sklenar et al., 1994). The independent assignments of potential nitrogen hydrogen bond acceptor sites using the intraresidue ^{2}J(H2,N1), ^{2}J(H2,N3), and ^{2}J(H8,N7) correlations for the purine residues in the ScYLV RNA pseudoknot were obtained from a two-bond ^{2}J(H,N) ^{1}H,^{15}N-HSQC experiment shown in Figure 6. Optimal sensitivity for the investigation of N1, N3 and N7 hydrogen bond acceptor sites in purines can be achieved by tuning the corresponding

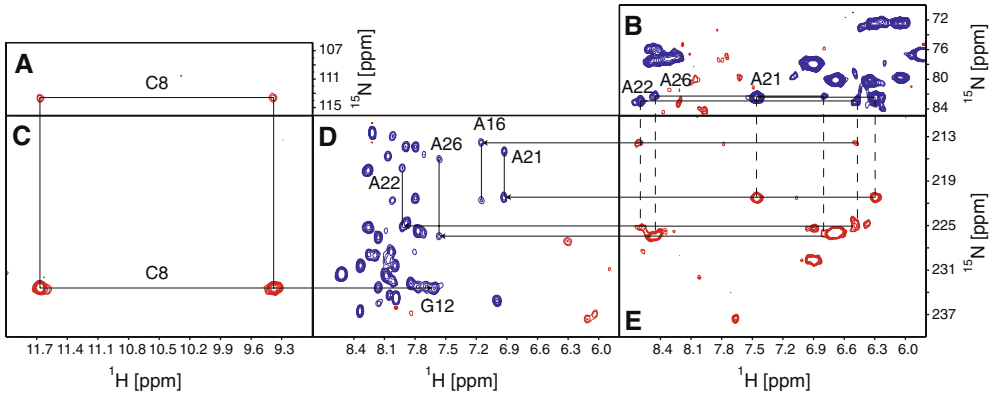

Figure 6. Observable major groove and minor groove amino proton correlations in a single quantitative, adiabatic *J*(N,N) HNN-COSY experiment. (A) HNN-COSY reference C8+ N4 (113.95 ppm) to amino H42 (11.66 ppm) and H41 (9.33 ppm) cross peaks. (B) HNN-COSY reference peaks correlating adenosine amino N6 nitrogen and amino H61/2 proton resonances. (C) HNN-COSY cross peaks showing C8+ amino H41/2 proton to G12 N7 nitrogen correlations mediated by ^{h2}J(N3,N7), see Figure 2A. (D) Independent two-bond ^{2}J(H,N)-HSQC showing purine H8 to N7 correlation and adenosine H2 to N1/N3 correlations (connected by vertical, solid lines). Nitrogen proton acceptor sites G12, A16, A21, A22, and A26 are assigned. (E) HNN-COSY cross peaks via ^{2}J(N6,N1) showing correlations of adenosine amino H61/2 protons to the N1 nitrogen of the same nucleobase (vertical, dashed lines). In the case of A22, the amino protons show additional correlations to the acceptor N3 nitrogen of A16 mediated by ^{h2}J(N6,N3), see Figure 2D.

INEPT delay to approximately 25 ms (25 ms $< 1/2J$; $J = {}^{2}J$(H8,N7) + ^{2}J(H8,N9) or ^{2}J(H2,N1) + ^{2}J(H2,N3)).

For the two-bond ^{2}J(H,N) ^{1}H,^{15}N-HSQC experiment, 64 complex points were recorded with an acquisition time of 14.8 ms for ^{15}N (ω_1), and 1024 complex points with an acquisition time of 93.5 ms for ^{1}H (ω_2). A repetition delay between transients of 1.5 s was used, with 48 scans per increment (total measuring time 3 h).

Quantitative J(H,N) ^{1}H,^{15}N-HSQC

For the quantitative *J*(H,N) ^{1}H,^{15}N-HSQC experiment (Dingley et al., 1999), 128 complex points were recorded with an acquisition time of 12.4 ms for ^{15}N (ω_1), and 2048 complex points with an acquisition time of 75.7 ms for ^{1}H (ω_2). A repetition delay between transients of 1.5 s was used, with 16 scans per increment (total measuring time 2 h) for the reference experiment (correlations arise predominantly from intranucleotide ^{1}J(H,N) couplings) and 128 scans per increment (total measuring time 16 h) for the cross experiment (correlations arise predominantly from magnetization transfer across the hydrogen bond through ^{h1}J(H,N) couplings). These two experiments were recorded on a four-channel Varian Inova 600 MHz spectrometer equipped with an actively shielded *z*-gradient triple-resonance probe, at a temperature of 298 K.

Quantification of $^{n}J(N,N)$ coupling constants using the adiabatic HNN-COSY

After the excitation of the exchangeable imino- and amino-protons employing the pulses sequence shown in Figure 3B, an INEPT transfer creates transverse ^{15}N magnetization. This ^{15}N source magnetization defocuses with respect to its long-range ^{15}N coupling partner during a tunable period $\tau = 38$–46 ms. It should be noted that the total length of the adiabatic [CHIRP-21,42,21] pulse needs to be added to τ in order to account for *J*(N,N) coupling evolution during the pulse. The fraction of magnetization giving rise to the reference peak intensity is proportional to $\cos(\pi J_{NsNd}\tau)\Pi_k\cos(\pi J_{NsNk}\tau)$, k $\neq$ s, d, where the index s characterizes the source ^{15}N nuclei while the index d characterizes the scalar coupled destination ^{15}N nuclei. Similarly, the transfer function of magnetization giving rise to the cross peak intensity is proportional to $\sin(\pi J_{NsNd}\tau)\Pi_k\cos(\pi J_{NsNk}\tau)$. After chemical shift evolution of the ^{15}N magnetization during t_1, the same fractions are refocused following the reverse pathway. Thus, the ratio of the transfer amplitudes of the reference and the cross peak intensity equals

$-\tan^2(\pi J_{\mathrm{NsNd}}\tau)$ (Bax et al., 1994). Because the line shapes of the cross and the reference signal are the same in ω_2 (^{1}H) and the line shape in the ω_1 (^{15}N) dimension is limited by digitization and the apodization function, values of ^nJ(Ns,Nd) can be derived from the intensity ratio, $I^{\mathrm{cross}}/I^{\mathrm{ref}} = -\tan^2(\pi J_{\mathrm{NsNd}}\tau)$. It should be noticed that only absolute values of $|^nJ(\mathrm{Ns,Nd})|$ can be determined by this method. The reported uncorrected coupling constant values may be systematically underestimated by up to 10% due to lower ^{15}N fractions (Kojima et al., 2000) and differential relaxation of ^{15}N in-phase and antiphase magnetization due to finite ^{15}N T_1 relaxation times during the defocusing periods τ (Harbison, 1993; Norwood, 1993; Norwood and Jones, 1993; Rexroth et al., 1995).

Quantification of $^nJ(H,N)$ coupling constants

Following the methodology introduced by Dingley et al., scalar ^nJ(H,N) couplings can be determined from quantitative J(H,N) ^{1}H,^{15}N-HSQC experiments (Dingley et al., 1999). As previously described, ^nJ(H,N) values are derived from the approximated expression $I^{\mathrm{cross}}/I^{\mathrm{ref}} \approx (2\pi J_{\mathrm{HsNd}}\delta)^2$. Again, only absolute values of $|^nJ(\mathrm{Hs,Nd})|$ can be determined by this method. As in the case of the HNN-COSY correlation, the quantitative J(H,N) ^{1}H,^{15}N-HSQC experiments is susceptible to lower ^{15}N isotopic abundance of the nitrogen coupling partner and differential relaxation effects.

Results and discussion

Cytidine and adenosine assignments

Although nearly complete resonance assignments for the ScYLV pseudoknot were acquired previously with standard methodologies (BMRB # bmr6509) (Cornish et al., 2005), it proved important to obtain and confirm the cytidine N3 and adenosine N1 resonances for residues not involved in Watson–Crick base pairs where *trans* hydrogen bond ^{h2}J(N,N) scalar couplings are not detected. In principal, cytidine N3 chemical shift assignments can be obtained following three different magnetization pathways.

The H5(C5C4)N3 experiment presented here correlates the non-exchangeable H5 of cytidine to N3 (Figure 4). This experiment is especially useful for cytidine residues not involved in Watson–Crick base pairs (C25 and C27). It was crucial in identifying the N3 resonance of cytidine C25 that is flipped out of the triple-stranded stack formed by L2. The solvent exposed amino protons of C25 are broadened beyond detection because of intermediate rotations around the exocyclic C4–N4 bond and, presumably by a combination of conformational and solvent exchange phenomena. These unfavorable properties necessitate detection on the non-exchangeable H5 proton.

An adiabatic HNN-COSY spectrum provided unambiguous assignments for cytidine via intraresidue correlation of the exchangeable amino H41 and H42 proton resonances to N3 (Figure 5D) mediated by ^2J(N4,N3) couplings. The same adiabatic HNN-COSY can also be used to establish N1 nitrogen assignments for adenosine residues where the amino H61 and H62 proton resonances are correlated to N1 nitrogens using the intrabase ^2J(N6,N1) couplings (Figures 5D, 6D). However, only three intrabase connectivities were easily observed for adenosines A21, A22, and A26, again attributable to unfavorable properties of H61/2 amino protons undergoing intermediate-to-fast rotations around the exocyclic C6–N6 bond and rapid exchange with the solvent (Mueller et al., 1995).

Finally, a quantitative J(H,N) ^{1}H,^{15}N-HSQC experiment can be used to establish cytidine N3 nitrogen assignments through intraresidue ^3J(H41,N3) scalar couplings with the added benefit of achieving sterospecific assignments of amino H41 and H42 protons. Typically, two distinct, non-degenerate resonance frequencies can be observed for the geminal amino protons of cytidine due to partially hindered rotation around the exocyclic C4–N4 bond. Cross peaks are only observed in the quantitative J(H,N) ^{1}H,^{15}N-HSQC experiments shown in Figure 5B when the amino proton H41 and the N3 nitrogen occupy a *trans* configuration; on the other hand, no correlations are observed that originate on the hydrogen-bonded *cis* H42 amino proton. The latter approach, pioneered by Tinoco and coworkers (Rudisser et al., 1999), was subsequently shown to be less sensitive than the adiabatic HNN-COSY when applied to a medium-sized RNA, which can mainly be attributed to the unfavorable T_2-relaxation properties of amino protons with respect to the corresponding nitrogen.

Spectroscopic characterization of the major groove triple base pair in the ScYLV RNA

A protonated C+·(G-C) major groove base triple is essential for the structure and function of all characterized luteoviral RNA pseudoknots including those derived from ScYLV and PEMV-1 (Figure 2A) (Su et al., 1999; Nixon et al., 2002a; Nixon et al., 2002b; Cornish et al., 2005; Pallan et al., 2005). Protonation of cytidine (C8 in ScYLV, C10 in PEMV-1) strongly stabilizes the RNA pseudoknotted structure by 1 to 3 kcal · mol^{-1} and elevates the pK_a of the protonated cytidine to >7.0 (Nixon et al., 2002a; Cornish et al., 2005). NMR investigation of these pseudoknots has shown that in addition to the cytidine H3 imino proton, the H41/2 amino protons of the protonated cytidine are shifted downfield (9–12 ppm; see Figure 6A, C) relative to cytidine amino protons involved in Watson–Crick base pairing (Nixon et al., 2002b; Cornish et al., 2005). It should be noted that the N3 resonance shifts upfield upon protonation to 140.85 ppm (Table 1). An adiabatic HNN-COSY experiment performed on the ScYLV RNA pseudoknot shows that the imino proton of C8+ does not have a nitrogen hydrogen bond acceptor consistent with a C8+H3···O6 G12 hydrogen bond. However, the same adiabatic HNN-COSY reveals that the amino protons of C8+ correlate to both N3 of C8+ via intraresidue two-bond transfer from N4 to N3 (data not shown) as well to the proton acceptor site N7 of G12, thereby establishing the presence of this tertiary hydrogen bond (Figure 6A, C). The analogous correlation was also present in the C10+ base triple of PEMV-1. For the ScYLV RNA, quantitative measurement of the ^{h2}J(N,N) coupling constant between C8+ N4 and G12 N7 yields 7.9 Hz (Table 1).

Spectroscopic characterization of the minor groove base triples

Previous functional, thermodynamic, and molecular dynamics experiments have established the importance of two *cis* Watson–Crick/sugar edge interactions at the 3′ end of L2 for stability and efficient functional activity in luteoviral RNA pseudoknots (Kim et al., 1999; Kim et al., 2000; Csaszar et al., 2001; Nixon et al., 2002a; Cornish et al., 2005). A quantitative 1D [^{15}N] Spin–Echo Difference experiment confirmed the A27 N1 to C15 2′-OH hydrogen bond in the PEMV-1 RNA pseudoknot with a ^{h1}J(2′-OH,N1) coupling constant of 1.7 ± 0.1 Hz (Giedroc et al., 2003). The ScYLV RNA pseudoknot contains the same two L2-S1 interactions except that the *cis* Watson–Crick/sugar edge interaction at the base of S1 is C27·(C14-G7) replacing the most 3′ L2 adenosine nucleotide with cytidine. The chemical shift dispersion of 2′-OH resonances within canonical A-form helices is limited, with resonance frequencies clustering between 6.75 and 7.00 ppm (Fohrer et al., 2006; Hennig et al., 2005). Our NMR spectra suggest that one diagnostic determinant for minor groove 2′-OH interactions involving electronegative acceptor atoms such as N1 or N3 nitrogens is a downfield shift of the 2′-OH resonance and marked protection from exchange with solvent. This observed downfield shift of the isotropic chemical shift of the hydrogen bonded 2′-OH hydroxyl proton reflects a decrease of the electron density around the nucleus and deshielding effects attributable to the nitrogen acceptor atom. The C27·(C14-G7) interaction is structurally analogous to the A27·(C15-G8) interaction in the PEMV-1 RNA except that the 2′-OH of C14 in the ScYLV RNA is shifted by ~1.3 ppm upfield relative to the 2′-OH in the PEMV-1 RNA. This shift in the 2′-OH chemical shift when adenosine or cytidine is in the terminal position of L2 was also observed in a mutational analysis of the ScYLV and BWYV RNA pseudoknots (Cornish et al., 2005). The noticeable chemical shift difference of 2′-OH hydroxyl protons that participate in *cis* Watson–Crick/sugar edge interactions most likely reflects distinct deshielding effects of the N1 (adenosine) vs. N3 (cytidine) nitrogen acceptor atoms, but the influence of hydrogen bond geometry may not be negligible. The A24·(C15-G6) base triple, the A22·(A16-U5), and the A21·(C17-G4) base triples (Figure 2) in the ScYLV RNA also have downfield shifted 2′-OH resonances relative to 2′-OH chemical shifts commonly observed in A-form helices (Cornish et al., 2005). Inspection of Figure 5B reveals that the C14 2′-OH to C27 N3 hydrogen bond is directly detectable due to the ^{h1}J(2′OH,N3) scalar coupling; however, quantitative measurement of the coupling constant could not be obtained. Unfortunately, the application of the quantitative 1D [^{15}N] Spin–Echo Difference experiment for ScYLV is hampered by severe

Table 1. Intrabase ^{2}J(N,N) and ^{3}J(H,N) couplings

	^{1}H (ppm) – H41/H42 & H61/H62	^{15}N (ppm) – N4/N6	^{15}N (ppm) – N3/N1	NN Coupling (Hz)	H41,N3 Coupling (Hz)
C8[a]	9.33, 11.66	113.95	140.85	2.1 ± 0.2	7.0 ± 0.5
C10	6.22, 8.28	96.35	197.20	5.1 ± 0.2	n.d.
C11	7.43, 7.96	97.17	194.80	4.4 ± 0.1	8.6 ± 0.7
C14	7.18, 8.44	95.44	197.49	4.7 ± 0.1	7.3 ± 0.2
C15	6.85, 8.67	97.94	194.87	4.7 ± 0.1	7.3 ± 0.2
C17	6.97, 8.02	97.67	198.01	4.6 ± 0.2	9.9 ± 0.4
C27	5.93, 7.30	95.92	199.06	5.2 ± 0.1	7.3 ± 0.2
A21	6.28, 7.42	82.55	221.56	4.5 ± 0.3	n.d.
A22[b]	6.49, 8.61	83.04	225.09	4.2 ± 0.2	n.d.

Trans hydrogen bond ^{h2}J(N,N) and ^{h1}J(H,N) couplings

	^{1}H (ppm) – H1, H3, & H41/H42	^{15}N (ppm) – donor	^{15}N (ppm) – acceptor	NN Coupling (Hz)	HN Coupling (Hz)
G4-C17	13.35	N1 – 148.10	N3 – 198.01	5.7 ±0.04	2.0 ± 0.1
U5-A16	14.06	N3 – 162.74	N1 – 221.93	7.0 ±0.02	1.7 ± 0.1
G6-C15	12.35	N1 – 146.44	N3 – 194.82	6.2 ±0.02	1.6 ± 0.1
G7-C14	13.22	N1 – 148.06	N3 – 197.45	5.7 ±0.01	2.1 ± 0.1
G12-C28	13.62	N1 – 147.61	N3 –195.16	6.5 ± 0.1	<0.9
U18-A3	14.12	N3 – 161.31	N1 – 221.99	6.2 ±0.1	<1.5
G29-C11	12.70	N1 – 146.27	N3 –194.71	6.3 ± 0.03	2.4 ± 0.2
G30-C10	12.62	N1 – 146.94	N3 –197.31	5.6 ± 0.6	<3.3
C8-G12	9.33, 11.66	N4 – 113.95	N7 – 233.56	7.9 ± 0.3	n.d.
A22-A16[b]	6.49, 8.61	N6 – 83.04	N3 – 213.91	4.4 ± 0.3	n.d.

^{1}H chemical shifts were externally referenced to DSS, with ^{15}N and nitrogen shifts referenced indirectly according to ^{15}N/^{1}H chemical shift ratios (Wishart et al., 1995). Experimental J(N,N) and J(H,N) coupling values are extracted from the quantitative, adiabatic J_{NN} HNN-COSY (500 MHz proton resonance frequency) and the quantitative J_{HN}^{1}H,^{15}N HSQC (600 MHz proton resonance frequency), respectively. J(N,N) coupling constants correspond to averages from three independent experiments carried out with varying J-defocusing delays of 40.8, 44.8, and 48.8 ms unless indicated. Reported errors correspond to standard deviations. J(H,N) coupling values were derived from a single experiment with a J-defocusing delays of 22.9 ms. Upper limits for ^{1h}J(H,N) couplings were derived for correlations beyond the detection limit from the noise level of the experiment. All measurements were carried out at 25 °C unless indicated.

[a] J(N,N) coupling derived from single measurement with J-defocusing delay of 40.8 ms, detected as C8^{+}N3 (diagonal peak) to C8^{+}N4 (cross peak) combination (error estimated from the spectral noise level).

[b] Single measurement with J-defocusing delay of 44.8 ms, carried out at 15 °C (error estimated from the spectral noise level).

[n.d.] Not determined due to undetectable diagonal peaks.

resonance overlap of the 2′-OH of C14 with aromatic and amino protons. Additionally, direct N1 to 2′-OH correlations mediated by *trans* hydrogen bond scalar couplings could not be detected for the A24·(C15-G6), the A22·(A16-U5), and the A21·(C17-G4) adenosine minor groove interactions. This can likely be attributed to small ^{h1}J(2′OH,N1) couplings, insufficient 2′-OH protection from exchange with solvent, resonance overlap of the 2′-OH with aromatic and amino protons or any combination thereof.

The exocyclic amino groups of adenosines and guanosines involved in canonical Watson–Crick base pairs are typically affected by intermediate-to-fast rotation around the C–N bond resulting in a single, degenerate proton resonance frequency (Mueller et al., 1995). Solvent exchange rates and the conformational dynamics of adenosine H61/2 amino protons often prevent their observation with the exception of lower temperature studies. However, the amino protons of A21, A22, A23, A24, and A26 in the ScYLV RNA are well protected from exchange even at 25 °C, conditions where the amino protons of A16, which is involved in a Watson–Crick base pair, are not observed (Cornish et al., 2005). Additionally, the amino protons of L2 adenosines involved in the nearly continuous stack formed in the minor groove of S1 (A21, A22, and A26) show non-degenerate resonance frequencies for H61 and H62 protons, respectively, indicating substantially hindered rotation around the C–N bond as a consequence of hydrogen bonding interactions. We did not attempt to obtain direct evidence for the Ade L2 N6···O2 Cyt S1 hydrogen bonds. Scalar couplings of the type ^{h3}J(N,C) in hydrogen bonded N–H···O=C systems have been reported in guanosine quartets, but are inevitably extremely small ($<<1$ Hz) (Liu et al., 2000b). However, scalar coupling for the more favorable A22 N6–A16 N3 hydrogen bond was indeed observed (4.4 Hz, Figure 6D and Table 1) thereby providing direct evidence for the presence of this particular hydrogen bond.

^{n}J(N,N) and ^{n}J(H,N) coupling measurement

A quantitative version of the adiabatic HNN-COSY experiment at 500 MHz provides for the measurement of J(N,N) for Watson–Crick base pairs, tertiary internucleotide structural interactions, as well as intrabase cytidine and adenosine couplings (Table 1). A J(H,N) ^{1}H,^{15}N-HSQC at 600 MHz provides J(H,N) couplings for many of the same interactions (Table 1). Intrabase cytidine ^{2}J(N,N) range from 4.2 to 5.2 Hz except for C8+, which exhibits a coupling constant of 2.1 Hz. This measured coupling for C8+, which is at least 2 fold less than all other cytidine couplings in the ScYLV RNA can be attributed to the altered electronic environment resulting from protonation. The corresponding ^{3}J(H,N) couplings ranged from 7.0 Hz, observed for C8+, to 9.9 Hz (Table 1). The latter intraresidue scalar couplings allow for stereospecific assignments of the cytidine amino protons, H41 and H42. Inevitably, the upfield shifted H41 showed correlations mediated by ^{3}J(H41,N3) couplings (Rudisser et al., 1999). Only two ^{2}J(N6,N1) adenosine intrabase couplings were measured (A21, A22) and these range from 4.2 to 4.5 Hz (Table 1). The corresponding amino proton to N1 nitrogen correlations via ^{3}J(H,N) couplings were not observed, presumably due to fast proton T_2-relaxation, small intraresidue ^{3}J(H,N) couplings, or a combination of both.

Trans hydrogen bond ^{h2}J(N,N) scalar coupling constants were measured for all eight canonical Watson–Crick base pairs and range from 5.6 to 7.0 Hz. In addition, ^{h1}J(H,N) scalar couplings were also measured for five of the Watson–Crick base pairs with upper limits obtained for the other three (Table 1). The shorter r(N1...N3) distances in canonical A-U base pairs as compared to G-C base pairs coincide with slightly larger ^{h2}J(N,N) couplings, in agreement with previous studies (Dingley and Grzesiek, 1998; Pervushin et al., 1998). As mentioned, the largest ^{h2}J(N,N) scalar coupling measured was 7.9 Hz for the C8+ H3 to G12 N7 hydrogen bond. The values for the *trans* hydrogen bond ^{h1}J(H,N) scalar coupling constants observed for the Watson–Crick base pairs range from approximately 1.6 to 2.4 Hz.

Conclusions

The two major intrinsic driving forces of RNA tertiary structure formation are base stacking and edge-to-edge interactions between nucleobases. Additionally, edge-to-edge parings in the minor groove frequently involve the 2′-OH hydroxyl

group of the ribose. The edge-to-edge interactions are predominantly electrostatic in nature and rely on a complementary arrangement of hydrogen bond donor and acceptor atoms (Lee and Gutell, 2004; Leontis et al., 2002). Commonly occurring canonical base pairs link the two interacting bases by two or three hydrogen bonds, thus leaving a number of potential hydrogen bond donor and acceptor sites accessible. The puzzling variety of possible interactions still makes predictions of complex RNA tertiary structure a daunting task (Batey et al., 1999; Westhof and Fritsch, 2000). NMR already has proved a capable tool for the unambiguous identification of N–H···N, N–H···O, O–H···N, and O–H···O hydrogen bonds and new experiments for their detection promise to become particularly useful (Dingley et al., 2001; Grzesiek et al., 2001).

In this report, we present a quantitative adiabatic HNN-COSY experiment that may provide a general strategy to observe hydrogen bonding interactions in oligonucleotides where donor and acceptor nitrogens are separated by up to 140 ppm. Our broadband HNN-COSY experiment opens up new pathways for magnetization transfer within nucleobases as well as for the characterization of N–H···N hydrogen bonds, analogous to the hydrogen bonds between exocyclic amino nitrogen donor and aromatic nitrogen acceptor sites observed here. In favorable cases, the unambiguous identification of hydrogen bonding partners allows for the introduction of additional distance restraints between donor and acceptor functional groups. This is especially important for RNA structure determination due to the relative paucity of protons in this environment. We also present complementary methods to obtain unambiguous chemical shift assignments of crucial N3 nitrogen resonances in cytidine residues. The adiabatic HNN-COSY experiment correlates the N3 hydrogen bond acceptor site with the amino N4 nitrogen via intrabase ^{2}J(N4,N3) couplings; a connectivity between the N3 nitrogen and the *trans* H41 amino proton can be established using ^{3}J(H41,N3) couplings in quantitative J(H,N) ^{1}H,^{15}N-HSQC experiments. Lastly, the triple-resonance H5(C5C4)N3 experiment links the cytidine N3 nitrogen resonances with the non-exchangeable H5 proton in cases where the H41 and H42 amino protons are not available for direct detection.

Acknowledgements

M. H. thanks Dr. Wolfgang Bermel for fruitful discussions. Financial support from the National Institutes of Health (AI040187) is gratefully acknowledged. P. V. C. was supported in part by a predoctoral Chemistry-Biology Interface Training Grant (T32 GM08523) to Texas A&M University.

References

Barfield, M., Dingley, A.J., Feigon, J. and Grzesiek, S. (2001) *J. Am. Chem. Soc.*, **123**, 4014–4022.
Batey, R.T., Rambo, R.P. and Doudna, J.A. (1999) *Angew Chem. Int. Edit.*, **38**, 2327–2343.
Bax, A., Ikura, M., Kay, L.E. and Zhu, G. (1991) *J. Magn. Reson.*, **91**, 174–178.
Bax, A., Vuister, G.W., Grzesiek, S., Delaglio, F., Wang, A.C., Tschudin, R. and Zhu, G. (1994) *Methods Enzymol.*, **239**, 79–105.
Benedict, H., Shenderovich, I.G., Malkina, O.L., Malkin, V.G., Denisov, G.S., Golubev, N.S. and Limbach, H.H. (2000) *J. Am. Chem. Soc.*, **122**, 1979–1988.
Bohlen, J.M. and Bodenhausen, G. (1993) *J. Magn. Reson. Ser. A*, **102**, 293–301.
Cornish, P.V., Hennig, M. and Giedroc, D.P. (2005) *Proc. Natl. Acad. Sci. USA*, **102**, 12694–12699.
Csaszar, K., Spackova, N., Stefl, R., Sponer, J. and Leontis, N.B. (2001) *J. Mol. Biol.*, **313**, 1073–1091.
Del Bene, J.E., Perera, S.A. and Bartlett, R.J. (1999) *J. Phys. Chem. A*, **103**, 8121–8124.
Delaglio, F., Grzesiek, S., Vuister, G.W., Zhu, G., Pfeifer, J. and Bax, A. (1995) *J. Biomol. NMR*, **6**, 277–293.
Dingley, A.J., Cordier, F. and Grzesiek, S. (2001) *Concepts Magn. Reson.*, **13**, 103–127.
Dingley, A.J. and Grzesiek, S. (1998) *J. Am. Chem. Soc.*, **120**, 8293–8297.
Dingley, A.J., Masse, J.E., Feigon, J. and Grzesiek, S. (2000) *J. Biomol. NMR*, **16**, 279–289.
Dingley, A.J., Masse, J.E., Peterson, R.D., Barfield, M., Feigon, J. and Grzesiek, S. (1999) *J. Am. Chem. Soc.*, **121**, 6019–6027.
Du, Z., Giedroc, D.P. and Hoffman, D.W. (1996) *Biochemistry*, **35**, 4187–4198.
Emsley, L. and Bodenhausen, G. (1990) *Chem. Phys. Lett.*, **168**, 297–303.
Emsley, L. and Bodenhausen, G. (1992) *J. Magn. Reson.*, **97**, 135–148.
Fiala, R., Munzarova, M.L. and Sklenar, V. (2004) *J. Biomol. NMR*, **29**, 477–490.
Fohrer, J., Hennig, M. and Carlomagno, T. (2006) *J. Mol. Biol.*, **356**, 280–287.
Furtig, B., Richter, C., Bermel, W. and Schwalbe, H. (2004) *J. Biomol. NMR*, **28**, 69–79.
Giedroc, D.P., Cornish, P.V. and Hennig, M. (2003) *J. Am. Chem. Soc.*, **125**, 4676–4677.
Giedroc, D.P., Theimer, C.A. and Nixon, P.L. (2000) *J. Mol. Biol.*, **298**, 167–185.
Grzesiek, S. and Bax, A. (1993) *J. Am. Chem. Soc.*, **115**, 12593–12594.

Grzesiek, S., Cordier, F. and Dingley, A.J. (2001) *Methods Enzymol*, **338**, 111–133.
Harbison, G.S. (1993) *J. Am. Chem. Soc.*, **115**, 3026–3027.
Hennig, M., Fohrer, J. and Carlomagno, T. (2005) *J. Am. Chem. Soc.*, **127**, 2028–2029.
Hennig, M. and Williamson, J.R. (2000) *Nucleic Acids Res.*, **28**, 1585–1593.
Hwang, T.L., van Zijl, P.C.M. and Garwood, M. (1997) *J. Magn. Reson.*, **124**, 250–254.
Jeffrey, G.A. and Saenger, W. (1991) *Hydrogen Bonding in Biological Structures*. Springer-Verlag, Berlin, New York.
Kawahara, S., Kojima, C., Taira, K. and Uchimaru, T. (2003) *Helv. Chim. Acta*, **86**, 3265–3273.
Kim, Y.C., Su, L., Maas, S., O'Neill, A. and Rich, A. (1999) *Proc. Natl. Acad. Sci. USA*, **96**, 14234–14239.
Kim, Y.G., Maas, S., Wang, S.C. and Rich, A. (2000) *RNA*, **6**, 1157–1165.
Kojima, C., Ono, A. and Kainosho, M. (2000) *J. Biomol. NMR*, **18**, 269–277.
Kolk, M.H., van der Graaf, M., Wijmenga, S.S., Pleij, C.W., Heus, H.A. and Hilbers, C.W. (1998) *Science*, **280**, 434–438.
Kupce, E. (2001) *Methods Enzymol.*, **338**, 82–111.
Lee, J.C. and Gutell, R.R. (2004) *J. Mol. Biol.*, **344**, 1225–1249.
Leontis, N.B., Stombaugh, J. and Westhof, E. (2002) *Nucleic Acids Res.*, **30**, 3497–3531.
Leontis, N.B. and Westhof, E. (2001) *RNA*, **7**, 499–512.
Liu, A., Hu, W.D., Qamar, S. and Majumdar, A. (2000a) *J. Biomol. NMR*, **17**, 55–61.
Liu, A.Z., Majumdar, A., Hu, W.D., Kettani, A., Skripkin, E. and Patel, D.J. (2000b) *J. Am. Chem. Soc.*, **122**, 3206–3210.
Majumdar, A., Kettani, A. and Skripkin, E. (1999a) *J. Biomol. NMR*, **14**, 67–70.
Majumdar, A., Kettani, A., Skripkin, E. and Patel, D.J. (1999b) *J. Biomol. NMR*, **15**, 207–211.
Marion, D., Ikura, M., Tschudin, R. and Bax, A. (1989) *J. Magn. Reson.*, **85**, 393–399.
Mueller, L., Legault, P. and Pardi, A. (1995) *J. Am. Chem. Soc.*, **117**, 11043–11048.
Nixon, P.L., Cornish, P.V., Suram, S.V. and Giedroc, D.P. (2002a) *Biochemistry*, **41**, 10665–10674.
Nixon, P.L., Rangan, A., Kim, Y.G., Rich, A., Hoffman, D.W., Hennig, M. and Giedroc, D.P. (2002b) *J. Mol. Biol.*, **322**, 621–633.
Norwood, T.J. (1993) *J. Magn. Reson. Ser. A*, **101**, 109–112.
Norwood, T.J. and Jones, K. (1993) *J. Magn. Reson. Ser. A*, **104**, 106–110.
Pallan, P.S., Marshall, W.S., Harp, J., Jewett, F.C., Wawrzak, Z., Brown, B.A., Rich, A. and Egli, M. (2005) *Biochemistry*, **44**, 11315–11322.
Pervushin, K., Ono, A., Fernandez, C., Szyperski, T., Kainosho, M. and Wuthrich, K. (1998) *Proc. Natl. Acad. Sci. USA*, **95**, 14147–14151.
Piotto, M., Saudek, V. and Sklenar, V. (1992) *J. Biomol. NMR*, **2**, 661–665.
Pleij, C.W.A. (1994) *Curr. Opin. Struct. Biol.*, **4**, 337–344.
Pleij, C.W.A., Rietveld, K. and Bosch, L. (1985) *Nucleic Acids Res.*, **13**, 1717–1731.
Puglisi, J.D., Wyatt, J.R. and Tinoco, I. Jr. (1990) *J. Mol. Biol.*, **214**, 437–453.
Rexroth, A., Schmidt, P., Szalma, S., Geppert, T., Schwalbe, H. and Griesinger, C. (1995) *J. Am. Chem. Soc.*, **117**, 10389–10390.
Rudisser, S., Pelton, J.G. and Tinoco, I. (1999) *J. Biomol. NMR*, **15**, 173–176.
Scheurer, C. and Bruschweiler, R. (1999) *J. Am. Chem. Soc.*, **121**, 8661–8662.
Shaka, A.J., Barker, P.B. and Freeman, R. (1985) *J. Magn. Reson.*, **64**, 547–552.
Shaka, A.J., Keeler, J. and Freeman, R. (1983) *J. Magn. Reson.*, **53**, 313–340.
Shen, L.X. and Tinoco, I. Jr. (1995) *J. Mol. Biol.*, **247**, 963–978.
Sklenar, V., Peterson, R.D., Rejante, M.R. and Feigon, J. (1994) *J. Biomol. NMR*, **4**, 117–122.
Su, L., Chen, L.Q., Egli, M., Berger, J.M. and Rich, A. (1999) *Nat. Struct. Biol.*, **6**, 285–292.
Westhof, E. and Fritsch, V. (2000) *Struct. Fold Des.*, **8**, R55–R65.
Wijmenga, S.S. and van Buuren, B.N.M. (1998) *Prog. Nucl. Magn. Reson. Spectrosc.*, **32**, 287–387.
Wilkens, S.J., Westler, W.M., Weinhold, F. and Markley, J.L. (2002) *J. Am. Chem. Soc.*, **124**, 1190–1191.
Wishart, D.S., Bigam, C.G., Yao, J., Abildgaard, F., Dyson, H.J., Oldfield, E., Markley, J.L. and Sykes, B.D. (1995) *J. Biomol. NMR*, **6**, 135–140.
Wohnert, J., Dingley, A.J., Stoldt, M., Gorlach, M., Grzesiek, S. and Brown, L.R. (1999) *Nucleic Acids Res.*, **27**, 3104–3110.
Wohnert, J., Gorlach, M. and Schwalbe, H. (2003) *J. Biomol. NMR*, **26**, 79–83.
Zhu, G., Torchia, D.A. and Bax, A. (1993) *J. Magn. Reson. Ser. A*, **105**, 219–222.